Nucleon form factors in dispersively improved chiral effective field theory: Scalar form factor

J. M. Alarcón* and C. Weiss†
Theory Center, Jefferson Lab, Newport News, Virginia 23606, USA
(Received 2 August 2017; published 20 November 2017)

We propose a method for calculating the nucleon form factors (FFs) of G-parity-even operators by combining chiral effective field theory (χEFT) and dispersion analysis. The FFs are expressed as dispersive integrals over the two-pion cut at $t > 4M_\pi^2$. The spectral functions are obtained from the elastic unitarity condition and expressed as products of the complex $\pi\pi \to N\bar{N}$ partial-wave amplitudes and the timelike pion FF. χEFT is used to calculate the ratio of the partial-wave amplitudes and the pion FF, which is real and free of $\pi\pi$ rescattering in the t channel (N/D method). The rescattering effects are then incorporated by multiplying with the squared modulus of the empirical pion FF. The procedure results in a marked improvement compared to conventional χEFT calculations of the spectral functions. We apply the method to the nucleon scalar FF and compute the scalar spectral function, the scalar radius, the t-dependent FF, and the Cheng-Dashen discrepancy. Higher-order chiral corrections are estimated through the πN low-energy constants. Results are in excellent agreement with dispersion-theoretical calculations. We elaborate several other interesting aspects of our method. The results show proper scaling behavior in the large-N_c limit of QCD because the χEFT calculation includes N and Δ intermediate states. The squared modulus of the timelike pion FF required by our method can be extracted from lattice QCD calculations of vacuum correlation functions of the operator at large Euclidean distances. Our method can be applied to the nucleon FFs of other operators of interest, such as the isovector-vector current, the energy-momentum tensor, and twist-2 QCD operators (moments of generalized parton distributions).

DOI: 10.1103/PhysRevC.96.055206

I. INTRODUCTION

A. Form factors and dispersion relations

Form factors (FFs) are the most basic expressions of the nucleon's complex internal structure and finite spatial extent. They parametrize the transition matrix elements of local operators between nucleon states with different momenta and can be related to the spatial distribution of the corresponding physical quantities in localized nucleon states [1,2]. The most widely studied FFs are those of the conserved vector and axial vector currents (spin-1 operators), which describe the interaction of the nucleon with electromagnetic and weak external fields. The nucleon vector FFs are measured in elastic electron scattering experiments and are generally known well [3]; on the axial FFs, limited information is available from neutrino scattering and other sources [4]. Besides the conserved currents, there are many more local operators of interest for nucleon structure in the context of QCD. The quark and gluon scalar operators (spin-0 operators) represent the trace of the QCD energy-momentum tensor and measure the contribution of quark and gluon fields to the nucleon mass; they also govern the coupling of the nucleon to the Higgs boson [5]. The corresponding rank-2 traceless tensor operators (spin-2 operators) represent the traceless part of the QCD energy-momentum tensor and measure the momentum and angular momentum of quarks and gluons in the nucleon, as well as the forces acting on them [6–8]. A much larger class of local QCD operators (spin-n operators, $n \geqslant 1$) emerges in the QCD factorization of hard exclusive processes on the nucleon, in connection with the moments of the generalized parton distributions; see Refs. [9–12] for a review. Because all these operators couple to external fields that are not easily excited through scattering processes, little is known about the FFs from present experiments. It is therefore necessary to develop theoretical methods for calculating the nucleon FFs of such operators from first principles.

Dispersion relations have proven to be a useful tool in the theoretical analysis of nucleon FFs. They rely on the analytic properties of the FFs as functions of the invariant momentum transfer t and connect their behavior in the spacelike and timelike regions, $t < 0$ and $t > 0$. The FFs are represented as dispersive integrals over their cuts in the timelike region, which describe processes in which the operator couples to the nucleon through exchange of a hadronic system in the t channel. For G-parity-even operators, the hadronic state with the lowest mass is the $\pi\pi$ state, and the cut starts at $t > 4M_\pi^2$ (two-pion cut). Examples of such operators are the isovector-vector current, and the isoscalar-scalar and isoscalar-spin-2 operators. To evaluate the dispersive integrals, one needs to know the imaginary part of the FFs on the cut (spectral functions). The two-pion cut lies in the unphysical region below the $N\bar{N}$ threshold, where the spectral functions cannot be obtained from timelike nucleon FF data. In the case of the vector and scalar FFs, the spectral functions on the two-pion cut have been determined using amplitude analysis techniques with empirical input (unitarity relations with πN and $\pi\pi$ scattering data [13–17]; Roy-Steiner equations [18,19]). In order to make the dispersion relations predictive and to extend them to other operators of interest, one needs a theoretical method to calculate the spectral functions of the nucleon FFs.

Chiral effective field theory (χEFT) represents a systematic method for describing pion and nucleon structure and

*alarcon@jlab.org
†weiss@jlab.org

interactions in the low-energy, large-distance regime of strong interactions [20,21]; see Refs. [22–24] for a review. It is based on the effective dynamics resulting from the spontaneous breaking of chiral symmetry and allows one to calculate amplitudes at pion momenta $k_\pi \sim M_\pi$ in an expansion in M_π/Λ_χ with controlled accuracy ($\Lambda_\chi \sim 1\,\mathrm{GeV}$ represents the chiral symmetry breaking scale). The method has been applied to the spectral functions of the nucleon FFs on the two-pion cut, using either the relativistic or the heavy-baryon formulation for the nucleon degrees of freedom [25–29]. The χEFT results reproduce the empirical isovector-vector spectral functions at energies very near the two-pion threshold, $t - 4M_\pi^2 = \text{few } M_\pi^2$, but significantly underestimate the latter at larger energies $t \sim 10$–$50\ M_\pi^2$; see Ref. [29] for an explicit comparison. The reason for the discrepancy is the strong $\pi\pi$ rescattering in the t channel, which manifests itself in the ρ resonance at $t = 40\,M_\pi^2 = 0.77\,\mathrm{GeV}^2$ and results in an enhancement of the empirical spectral function. In χEFT, this effect is encoded in higher order $\pi\pi NN$ contact terms and pion loops and would appear in the form of large higher-order corrections, which makes the method impractical. A similar situation is observed in the spectral function of the scalar FF, where $\pi\pi$ rescattering does not produce a narrow resonance but is nevertheless strong. The limited reach of the χEFT calculations of the spectral functions precludes evaluation of the dispersion integral for the FFs based on χEFT input alone, as the contributions from larger t require separate modeling. In order to extend the reach of χEFT calculations of the spectral functions beyond the near-threshold region, one must find a way to account for $\pi\pi$ rescattering in the t channel more effectively.

In this article, we describe a new method that allows one to construct the spectral functions of FFs on the two-pion cut up to larger values of t (in practice, $t \lesssim 1\,\mathrm{GeV}^2$) and enables predictive dispersive calculations of the full nucleon FFs based on χEFT input alone. It uses the elastic unitarity condition for the $\pi\pi$ system in the t channel [13,14] and the N/D method of amplitude analysis [30]. The spectral function of the nucleon FF on the two-pion cut is expressed as the product of the $\pi\pi \to N\bar{N}$ t-channel partial-wave amplitude (PWA) and the complex-conjugate timelike pion FF. The two complex functions have same phase on the two-pion cut (Watson theorem) [31]. χEFT is used to calculate the ratio of the PWA and the timelike pion FF, which is real (it has no two-pion cut) and free of $\pi\pi$ rescattering effects. This function is then multiplied with the squared modulus of the empirical timelike pion FF, which contains the full $\pi\pi$ rescattering effects. The method results in a marked improvement compared to conventional "direct" calculations of the spectral functions in χEFT. Realistic spectral functions with controlled uncertainties are obtained up to $t \lesssim 1\,\mathrm{GeV}^2$. The basic idea was introduced in Ref. [32] in the context of a χEFT calculation of the nucleon's peripheral transverse densities (the Fourier transforms of the FFs) in the leading-order (LO) approximation. Here we describe the general method, include next-to-leading-order (NLO) chiral corrections (fixing of low-energy constants [LECs], convergence, uncertainty estimates) and demonstrate the potential for dispersive calculations of the FFs proper and their derivatives, which opens up a range of new applications. We also explore other interesting aspects of the new method. We point out a possible combination with first-principles calculations of the squared modulus of the timelike pion FF with Euclidean correlation functions (e.g., lattice QCD), which could be used for the dispersive calculation of FFs of QCD operators whose pion FFs are not known empirically. We demonstrate that our nucleon FF results have the correct scaling behavior in the large-N_c limit of QCD because the χEFT amplitudes include N and Δ intermediate states.

Here we apply the method to the nucleon scalar FF and its spectral function. The choice is motivated by pedagogical considerations and physical interest. The scalar density is the simplest operator, with only a single nucleon FF, and a single t-channel partial wave in the unitarity relation for the spectral function. The pion scalar FF has been determined from dispersion analysis with χEFT constraints and is available as input for our calculation [33–35]. The scalar nucleon FF has been computed using amplitude analysis techniques and serves as a reference point for our results [17,19]. The scalar FF thus represents the ideal testing ground for our method. It is also of great physical interest in itself, in connection with the nucleon mass problem and the coupling to the scalar sector of the standard model (see below). Applications of our method to the nucleon isovector-vector FFs will be presented in a forthcoming article [36].

The plan of this article is as follows. In the remainder of this section, we summarize the basic properties of the scalar FF and its dispersive representation. In Sec. II, we describe the general method of dispersively improved χEFT, including the elastic unitarity relation and N/D method, LO χEFT calculations, estimates of higher order corrections, and the properties of the pion FF. In Sec. III, we apply the method to the nucleon scalar spectral function and use it to calculate the nucleon scalar radius, the scalar FF, and the Cheng-Dashen discrepancy. In Sec. IV, we discuss the extraction of the timelike pion FF from Euclidean correlation functions and the correspondence of our approach with large-N_c QCD. An outlook on further applications is presented in Sec. V.

A combination of χEFT and dispersion theory similar to the one used here was proposed in the context of a recent study of hyperon transition FFs [37]. Techniques related to the N/D method were also applied in earlier χEFT studies of meson-meson, meson-baryon, and baryon-baryon scattering [38–44].

B. Scalar form factor

The scalar density of light quarks in QCD is measured by the composite local operator

$$O_\sigma(x) \equiv \hat{m} \sum_{f=u,d} \bar{\psi}_f(x)\psi_f(x), \tag{1}$$

where $\psi_f(x)(f = u,d)$ is the quark field and $\hat{m} \equiv m_u = m_d$ the quark mass (we assume isospin symmetry). The operator Eq. (1) is scale independent and represents the quark mass term in the QCD Lagrangian and Hamiltonian densities. The same operator appears in the trace of the QCD energy-momentum tensor, alongside the gluonic and strange-quark scalar operators and a similar light-quark operator that results

from the trace anomaly; see Ref. [5] for details. The transition matrix element of the operator Eq. (1) between nucleon states with 4-momenta p and p' is of the form

$$\langle N(p',s')|\, O_\sigma(0)\, |N(p,s)\rangle = \bar{u}' u \sigma(t), \tag{2}$$

where $\bar{u}' \equiv \bar{u}(p',s')$ and $u \equiv u(p,s)$ are the nucleon 4-spinors, and $\sigma(t)$ is the nucleon scalar FF. It is a function of the invariant momentum transfer $t \equiv (p'-p)^2$, with $t<0$ in the physical region of the nucleon transition (spacelike FF). The corresponding timelike FF is defined analogously, as the matrix element between the vacuum and a nucleon-antinucleon state, with $t \equiv (p'+p)^2 > 0$. The matrix elements are diagonal in isospin (N = proton, neutron).

The scalar FF is an analytic function of t. The physical sheet has cuts along the positive real axis, which result from processes in which the operator creates a hadronic state that couples to the $N\bar{N}$ system,

$$\text{operator} \to \text{hadronic state} \to N\bar{N}; \tag{3}$$

such processes occur in the unphysical region below the $N\bar{N}$ threshold. The lowest mass hadronic state with scalar quantum numbers is the $\pi\pi$ state with threshold at $t = 4M_\pi^2$ (two-pion cut); other hadronic states (4π etc.) give rise to further cuts with higher thresholds; the cuts can be combined to a principal cut starting at $t = 4M_\pi^2$. One can thus write dispersion relations that express the FF in the complex plane as an integral over the discontinuity on the principal cut. In practice, one considers a once-subtracted dispersion relation,

$$\sigma(t) = \sigma(0) + \frac{t}{\pi}\int_{4M_\pi^2}^{\infty} dt' \frac{\mathrm{Im}\,\sigma(t')}{t'(t'-t)}, \tag{4}$$

which suppresses contributions from large t' and ensures rapid convergence of the integral (see below). It determines the FF up to a subtraction constant, which is chosen as the value of the FF at $t=0$, $\sigma(0)$, the so-called pion-nucleon σ term. The integration is over the imaginary part of the FF on the principal cut, $\mathrm{Im}\,\sigma(t')$, which is referred to as the spectral function.

Of particular interest is the behavior of the scalar FF near $t=0$. The derivative of the FF at $t=0$ define the nucleon's scalar charge radius,

$$\langle r^2\rangle_\sigma \equiv \frac{6}{\sigma(0)}\frac{d\sigma}{dt}\bigg|_{t=0}. \tag{5}$$

The finite difference

$$\Delta_\sigma \equiv \sigma\left(t = 2M_\pi^2\right) - \sigma(t=0) \tag{6}$$

is needed in the extraction of the σ term from πN scattering data using the Cheng-Dashen theorem [45], which connects the Born-subtracted isoscalar πN scattering amplitude at $s = m_N^2$ and $t = 2M_\pi^2$ to $\sigma(t = 2M_\pi^2)$. The dispersive representation of these quantities is

$$\langle r^2\rangle_\sigma = \frac{6}{\pi\sigma(0)}\int_{4M_\pi^2}^{\infty} dt' \frac{\mathrm{Im}\,\sigma(t')}{t'^2}, \tag{7}$$

$$\Delta_\sigma = \frac{2M_\pi^2}{\pi}\int_{4M_\pi^2}^{\infty} dt' \frac{\mathrm{Im}\,\sigma(t')}{t'\left(t'-2M_\pi^2\right)}. \tag{8}$$

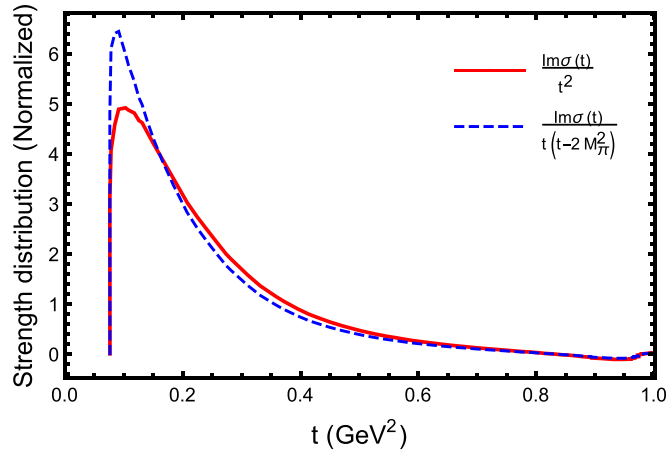

FIG. 1. Distribution of strength in the dispersive integrals for the scalar charge radius, Eq. (7) (solid red line), and the Cheng-Dashen discrepancy, Eq. (8) (dashed blue line). The plot shows the integrands as functions of t, divided by the value of the integral, i.e., normalized to unit area under the curves.

The convergence of these integrals at large t' is similar to that of the once-subtracted dispersion relation for the FF, Eq. (4).

The spectral function of the scalar nucleon FF has been constructed using amplitude analysis techniques with empirical input [17,19]. Figure 1 shows the distribution of strength in the dispersive integrals Eqs. (7) and (8). One sees that the integral converges rapidly and that the main contribution comes from the region $t' \lesssim 0.5\,\mathrm{GeV}^2$. This determines the range where one needs to calculate spectral functions if one aims for a first-principles calculation of the scalar quantities through their dispersive integrals.

Evaluation of the integrals with the empirical spectral functions of Ref. [17] has found $\langle r^2\rangle \sim 1.6\,\mathrm{fm}^2$, substantially larger than the proton's charge radius $\langle r^2\rangle_1 \sim 0.65\,\mathrm{fm}^2$ (Dirac radius). The discrepancy Δ_σ has been obtained at $\sim$14 MeV. The significance of these findings will be discussed in Sec. III.

The scalar FF of the pion is defined analogously to that of the nucleon in Eq. (2),

$$\langle \pi(p')|\, O_\sigma(0)\, |\pi(p)\rangle = \sigma_\pi(t), \tag{9}$$

where $\pi = \pi^+,\pi^-,\pi^0$ (isospin symmetry) and $t = (p'-p)^2 < 0$ in the physical region. The value at $t=0$ is

$$\sigma_\pi(0) = M_\pi^2, \tag{10}$$

which follows from the fact that the scalar operator corresponds to the chiral-symmetry-breaking pion mass term in the chiral Lagrangian. The corresponding timelike FF is defined as

$$\langle 0|\, O_\sigma(0)\, |\pi(p')\pi(p)\rangle = \sigma_\pi(t), \tag{11}$$

where now $t = (p+p')^2 > 4M_\pi^2$ in the physical region. The scalar FF of the pion is of physical interest in itself and enters in dispersive calculations of the nucleon scalar FF.

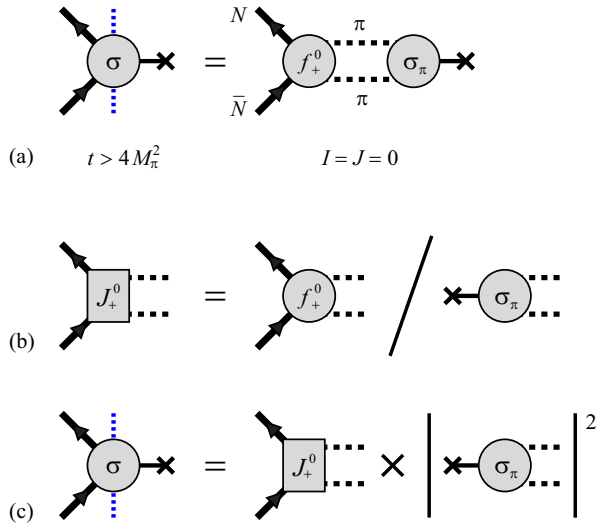

FIG. 2. (a) Unitarity relation for the imaginary part of the nucleon scalar FF on the two-pion cut, Eq. (12). (b) Real function $J^0_+(t)$, Eq. (16), defined as the ratio of the $\pi\pi \to N\bar{N}$ PWA and the pion FF. (c) Unitarity relation in terms of $J^0_+(t)$ and the squared modulus of the pion FF, Eq. (15).

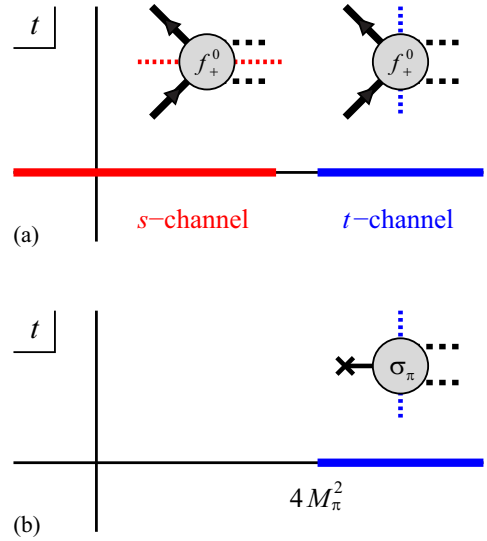

FIG. 3. (a) Analytic structure of the $\pi\pi \to N\bar{N}$ PWA. The function has a right-hand cut resulting from the t-channel $\pi\pi$ intermediate state and a left-hand cut resulting from s-channel intermediate states ($N, \Delta, \pi N$, ...). The phase of the PWA on the right-hand cut is the same as that of the pion FF. (b) Analytic structure of the pion FF. The function has a right-hand cut resulting from the $\pi\pi$ intermediate state.

II. METHOD

A. Dispersively improved χEFT

We now describe the method for calculating the spectral function of nucleon FFs on the two-pion cut in χEFT using a representation based on the elastic unitarity condition and the N/D method. While we use the scalar FF as a specific example, the method is general and can be applied to the FFs of any G-parity-even operator coupling to the $\pi\pi$ state.

In the region $4M_\pi^2 < t < 16M_\pi^2$, only the $\pi\pi$ state contributes to the discontinuity of the nucleon FF through the process Eq. (3). In this situation, the spectral function can be computed using the elastic unitarity condition, which expresses the conservation of flux in the t channel [13–15]. For the scalar nucleon FF, it takes the form [17]

$$\mathrm{Im}\,\sigma(t) = \frac{3k_{\mathrm{cm}}}{4\widetilde{p}_N^2\sqrt{t}} f_+^0(t)\,\sigma_\pi^*(t), \tag{12}$$

where

$$k_{\mathrm{cm}} \equiv \sqrt{t/4 - M_\pi^2} \tag{13}$$

is the center-of-mass momentum of the pions in the $\pi\pi$ system, and

$$\widetilde{p}_N \equiv \sqrt{m_N^2 - t/4} \tag{14}$$

is related to the unphysical momentum of the nucleons in the $N\bar{N}$ system [see Fig. 2(a)]. The function $f_+^0(t)$ is the $I = J = 0$ $\pi\pi \to N\bar{N}$ t-channel PWA, and $\sigma_\pi^*(t)$ is the complex conjugate of the timelike pion FF, Eq. (11). While the unitarity condition applies at real $t > 4M_\pi^2$ on the upper edge of the cut ($t \to t + i0$), the functions $f_+^0(t)$ and $\sigma_\pi(t)$ are defined for arbitrary complex t, and it is worthwhile to recall their analytic structure. The PWA $f_+^0(t)$ has both a right-hand cut and a left-hand cut [see Fig. 3(a)]. The right-hand cut results from t-channel processes with the $\pi\pi$ intermediate state and starts at $t = 4M_\pi^2$. The left-hand cut results from s-channel processes with intermediate baryonic states ($N, \Delta, \pi N$, ...) and starts at $t = 4M_\pi^2 - M_\pi^4/m_N^2$ for the intermediate N. The two cuts are thus of different physical origin. The pion FF $\sigma(t)$ has only a right-hand cut starting at $t = 4M_\pi^2$, resulting from the $\pi\pi$ intermediate state, which is just the two-pion cut of the pion FF [see Fig. 3(b)].

A crucial point is that the complex functions $f_+^0(t)$ and $\sigma_\pi(t)$ have the same phase on the right-hand cut (the two-pion cut). Physically, this follows from the fact that the phases of the two amplitudes arise from the same elastic $\pi\pi$ rescattering processes (Watson theorem) [31]. Mathematically, this is necessary for the product of $f_+^0(t)$ and $\sigma_\pi^*(t)$ to result in the real function $\mathrm{Im}\,\sigma(t)$, as was already implied in the unitarity condition Eq. (12). This circumstance allows one to rewrite the unitarity relation in a manifestly real form [13] [see Figs. 2(b) and 2(c)]:

$$\mathrm{Im}\,\sigma(t) = \frac{3k_{\mathrm{cm}}}{4\widetilde{p}_N^2\sqrt{t}} J_+^0(t)\,|\sigma_\pi(t)|^2, \tag{15}$$

$$J_+^0(t) \equiv \frac{f_+^0(t)}{\sigma_\pi(t)}. \tag{16}$$

The function $J_+^0(t)$ is real at $t > 4M_\pi^2$ and therefore has no right-hand cut; if it had one, there would be a discontinuity resulting in a nonzero imaginary part. It does have a left-hand cut, inherited from the PWA $f_+^0(t)$. The squared modulus $|\sigma_\pi(t)|^2$ is obviously real. The representation of Eqs. (15) and (16) permits a simple physical interpretation. Since the phase of $f_+^0(t)$ and $\sigma_\pi(t)$ arises from $\pi\pi$ rescattering processes, the equations effectively separate the $\pi\pi \to N\bar{N}$ coupling

[contained in $J_+^0(t)$, in which the phase cancels] from the $\pi\pi$ rescattering [contained in $|\sigma_\pi(t)|^2$, which is a purely pionic amplitude]. This interpretation can provide useful guidance for the following.

The representation of Eqs. (15) and (16) is equivalent to applying the N/D method to the $\pi\pi \to N\bar{N}$ PWA [30]. In this approach, the PWA is represented in the form $f_+^0(t) = N(t)/D(t)$, such that the right-hand cut (related to the t-channel exchanges) appears only in the factor $1/D(t)$, and the left-hand cut (related to the s-channel intermediate states) appears in the factor $N(t)$. In the case at hand, the D function is chosen as the inverse pion FF, $D(t) = 1/\sigma_\pi(t)$, and the N function is given by Eq. (16), $N(t) = J_+^0(t)$ [15].

The representation of Eqs. (15) and (16) suggests a new approach to calculating the spectral function of nucleon FFs on the two-pion cut in χEFT. We use χEFT to compute the real function $J_+^0(t)$ at $t > 4M_\pi^2$ to a fixed order. We then multiply the result with the empirical $|\sigma_\pi(t)|^2$, which contains the effects of $\pi\pi$ rescattering. This approach has several advantages compared to "direct" calculations of the nucleon spectral functions:

(a) The χEFT calculations of $J_+^0(t)$ are not affected by $\pi\pi$ rescattering, as the latter is contained entirely in $|\sigma_\pi(t)|^2$. The rescattering effects are strong and would require large higher-order corrections when treated within χEFT. We therefore expect the new approach to show much better convergence than direct χEFT calculations of the spectral function. Higher-order corrections can perturbatively improve the coupling of the $\pi\pi$ system to the nucleon described by $J_+^0(t)$, while the rescattering effects described by $|\sigma_\pi(t)|^2$ are taken from other sources (dispersion theory, data, lattice QCD).

(b) The organization according to Eqs. (15) and (16) is consistent with the idea of "separation of scales" basic to χEFT. The function $J_+^0(t)$ is dominated by the singularities of the N and Δ Born diagrams, or diagrams with πN inelastic intermediate states in higher orders, which are governed by the scales M_π and $m_\Delta - m_N$. The t dependence of the pion FF, in contrast, is governed by the chiral-symmetry-breaking scale $\Lambda_\chi \sim 1\,\text{GeV}$. The intrinsic logic of χEFT therefore suggests applying the χEFT calculations to $J_+^0(t)$ and treating $|\sigma_\pi(t)|^2$ as an external input.

(c) The timelike pion FF enters only through its squared modulus $|\sigma_\pi(t)|^2$, not its phase. This reduces model dependence in the determination of the empirical pion FF and represents an advantage over approaches working with the original unitarity condition, Eq. (12), where the pion FF enters as a complex function. The squared modulus of the timelike scalar pion FF can be extracted directly from Euclidean vacuum-to-vacuum correlation functions of the scalar operator, which can be computed in lattice QCD (see Sec. IV A). In the electromagnetic case, the squared modulus of the timelike pion FF can directly be measured in $e^+e^- \to \pi^+\pi^-$ exclusive annihilation experiments.

We refer to the new method as "dispersively improved χEFT" (DIχEFT). The method is applicable strictly at $4M_\pi^2 < t < 16\,M_\pi^2$, where only the $\pi\pi$ channel is open and the elastic unitarity condition Eq. (12) is valid. It is expected that inelasticities from other channels (4π) are small up to the $K\bar{K}$ threshold; by neglecting those, the representations of Eqs. (15) and (16) can effectively be used up to $t \sim 1\,\text{GeV}^2$. Our method could thus in principle be applied up to such values of t, provided that the χEFT calculations of $J_+^0(t)$ converge sufficiently well (this question will be investigated below).

B. Leading-order calculation

For the calculation of $J_+^0(t)$, we use SU(2)-flavor χEFT with relativistic N and Δ degrees of freedom. The relativistic formulation ensures the correct analytic structure of the amplitudes (position of branch points, threshold behavior), which is critical in the present application. The inclusion of the Δ as an explicit degree of freedom is needed because the Δ Born term makes important contributions to the $\pi\pi \to N\bar{N}$ PWA (see below); it is also needed to reproduce the correct scaling behavior of the spectral function in the large-N_c limit of QCD (see Sec. IV B). These features have proved to be essential also in other applications of baryon χEFT to πN scattering, photoproduction, and nucleon structure [46–56].

The basic setup of the relativistic χEFT used in the present study (fields, Lagrangian, power counting, couplings) is described in Ref. [57] and summarized in Ref. [32]. The spin-1/2 N is described by a relativistic bispinor field (Dirac field). The spin-3/2 Δ is introduced as a 4-vector-bispinor field, which has to be subjected to relativistically covariant constraints to eliminate spurious spin-1/2 degrees of freedom. Here we use the formulation in which the spin-1/2 degrees of freedom are allowed to propagate but are filtered out at the interaction vertices (consistent vertices) [58–61]. The construction of the chiral Lagrangian with the spin-3/2 fields has been described in Refs. [62,63]. Several expansion schemes have been proposed for the χEFT with the Δ, assuming certain parametric relations between the chiral parameters $k_\pi \sim M_\pi$ and the N-Δ mass splitting $m_\Delta - m_N$. In the present application, the differences between the various expansion schemes for the Δ are irrelevant, because the calculations are carried out at an accuracy where Δ loops do not enter. The only difference to χEFT with N only is in the appearance of the Δ Born graphs at leading order. We therefore denote the order of our calculations by LO, NLO, and N2LO, as is common in χEFT with N only.

Regarding the power counting, we note that χEFT calculations with relativistic baryons must in principle deal with power-counting-breaking terms arising from chiral loops with baryons, i.e., lower order terms in the chiral counting resulting from higher order terms in the loop expansion. The standard power counting for loops can be recovered by adopting the extended-on-mass-shell (EOMS) scheme [64]. While diagrams with chiral loops are not considered in the present study, it is important to mention this scheme here, as it ensures that the tree-level results are not mixed up with power-counting-breaking terms arising from chiral loops.

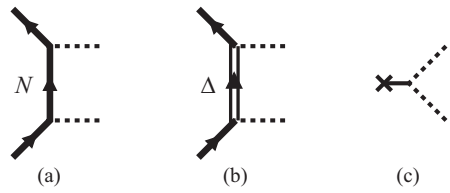

FIG. 4. [(a), (b)] LO χEFT diagrams contributing to the $\pi\pi \to N\bar{N}$ PWA. (c) Pion scalar FF in LO.

The LO χEFT diagrams for the $I = J = 0$ $\pi\pi \to N\bar{N}$ partial-wave amplitude $f_+^0(t)$ are the N Born term shown in Fig. 4(a) and the Δ Born term in Fig. 4(b); $\pi\pi NN$ contact terms appear only in higher orders and will be discussed below. In the LO calculation of the ratio $J_+^0(t)$, Eq. (16), the pion FF in the denominator is evaluated at LO; see Fig. 4(c). At this order in χEFT, the pion is pointlike, $\sigma_\pi(t) \equiv \sigma_\pi(0) = M_\pi^2$. The LO result for $J_+^0(t)$ is therefore just the result for $f_+^0(t)$ divided by M_π^2. At this accuracy, our approach based on Eq. (15) simply amounts to multiplying the LO χEFT result for the nucleon spectral function $\mathrm{Im}\,\sigma(t)$ (as obtained by direct χEFT calculation of the spectral function without the unitarity condition) by the normalized empirical pion FF $|\sigma_\pi(t)|^2/M_\pi^4$,

$$\mathrm{Im}\,\sigma(t) = \mathrm{Im}\,\sigma(t)\,[\mathrm{LO}]\,\frac{|\sigma_\pi(t)|^2}{M_\pi^4}. \tag{17}$$

This formula permits an extremely simple implementation of unitarity at LO accuracy. The factor $|\sigma_\pi(t)|^2/M_\pi^4$ describes the enhancement of the direct χEFT result for the spectral function due to $\pi\pi$ rescattering. Numerical results obtained with this approximation will be presented below.

The analytic expressions for the LO χEFT results for $J_+^0(t)$ are given in the appendix. The numerical values are shown in Fig. 5. For a better view, the plot shows the function multiplied by the kinematic factor of Eq. (15), $3k_{\mathrm{cm}}/(4\tilde{p}_N^2\sqrt{t})\,J_+^0(t)$; this combination is equal to $\mathrm{Im}\,\sigma(t)/|\sigma_\pi(t)|^2$ by virtue of Eq. (15). One observes that the contributions from the N and Δ Born term amplitudes have the same sign and are roughly comparable in magnitude.

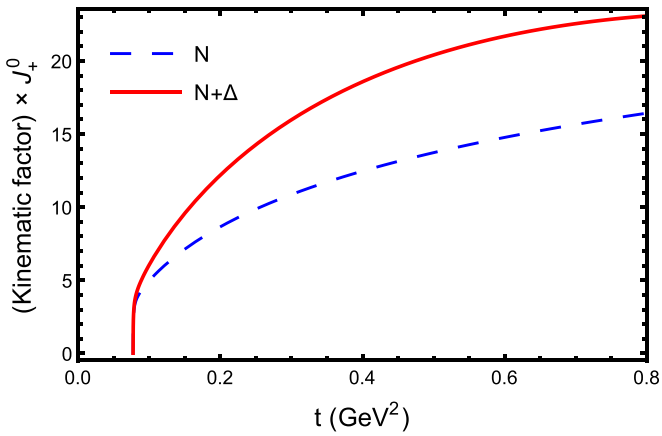

FIG. 5. LO χEFT result for the function $[3k_{\mathrm{cm}}/(4\tilde{p}_N^2\sqrt{t})]\,J_+^0(t)$, which enters in the manifestly real unitarity relation Eq. (15). Dashed blue line: Contribution of N Born term, Fig. 4(a). Solid red line: Sum of N and Δ Born terms, Figs. 4(a) and 4(b).

C. Estimates of higher-order corrections

At NLO accuracy, corrections to the πN scattering amplitude arise only from NLO $\pi\pi NN$ contact terms in the chiral Lagrangian. The NLO contributions to the $I = J = 0$ $\pi\pi \to N\bar{N}$ PWA in Eq. (16) therefore have simple structures. Corrections to the pion FF appear only at N2LO accuracy through pion loops. The expression for the NLO corrections to $J_+^0(t)$ is given in Eq. (A15) of the appendix. At this accuracy, Eq. (17) is still valid, and the NLO corrections to the spectral function are obtained simply by replacing $J_+^0(t)$ by its NLO expression.

For evaluating the higher-order corrections, we use the LECs of πN scattering. The values have to be adjusted consistently with the logic of our unitarity-based approach. The LECs in standard χEFT absorb rescattering effects that are treated explicitly within our unitarity-based approach. The contact terms appropriate for our approach are therefore obtained by subtracting the effects of rescattering from the original LECs. To do this in practice, we describe the rescattering effects in the $I = J = 0$ $\pi\pi$ channel through the σ meson exchange model of Ref. [65]. The resonance saturation hypothesis [66] then allows us to estimate how much of the original LECs is due to rescattering and subtract those amounts (see Fig. 6).

We take the NLO χEFT πN amplitude from Ref. [57] and perform the partial-wave projection according to the formulas of Ref. [13]. The LECs appearing in this amplitude at NLO have been determined through relativistic χEFT analysis of πN scattering with explicit Δ [57,67]. Performing the adjustment as described above, we obtain the values $c_i (i = 1,2,3)$ listed in Table III in the appendix. We use the parameters to evaluate the NLO contribution to $J_+^0(t)$ and estimate its uncertainty by varying the values in the determined range. Numerical results from this procedure will be shown below.

At N2LO accuracy, both the $\pi\pi \to N\bar{N}$ PWA and the pion FF involve loop corrections, and the structure of the χEFT expressions becomes considerably richer. At this order, $\pi\pi$ rescattering in the t channel occurs both in the PWA and in the pion FF, so that both functions become complex at $t > 4M_\pi^2$; one should therefore be able to verify explicitly that they have the same phase and that the phase cancels in the ratio in Eq. (16). Furthermore, at N2LO πN and $\pi\Delta$ s-channel intermediate states appear in the PWA and contribute to its

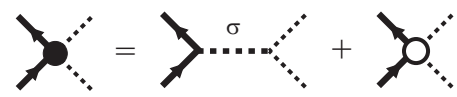

FIG. 6. Adjustment of the LECs of the NLO $\pi\pi NN$ contact term in our unitarity-based approach. The original contact term (filled circle, left-hand side) is equated with the sum of σ meson exchange and a reduced contact term (open circle). The reduced contact terms are used in the present scalar FF calculation with explicit unitarization.

left-hand cut. Here we do not pursue a full N2LO calculation of the function $J^0_+(t)$ including loops. Instead, we estimate the size of the N2LO corrections in a simple way, by using the N2LO tree-level result and varying the LECs in a meaningful range. To this end, we impose the unsubtracted dispersion relation for the scalar FF at $t = 0$ (σ term),

$$\sigma(0) = \frac{1}{\pi}\int_{4M_\pi^2}^{\infty} dt' \, \frac{\mathrm{Im}\,\sigma(t')}{t'}, \tag{18}$$

with the integration restricted to the region $t' < 1\,\mathrm{GeV}^2$. This relation fixes the LECs in the N2LO tree-level result in terms of $\sigma(0)$. We then generate an uncertainty band by varying $\sigma(0)$ in the range 45–59 MeV. The first value was determined in an earlier dispersive analysis of the σ term [68], while the second was obtained by χEFT from modern πN PWAs and pionic atom data [46], and supported by a subsequent analysis using Roy-Steiner equations [69]. Numerical results for $J^0_+(t)$ with these parameters will be shown below.

D. Pion form factor

For the pion scalar FF in Eq. (17), we take the result of the dispersive analysis of Ref. [35]; for earlier results, see Refs. [33,34]. The analysis includes the $K\bar{K}$ channel at $t > 1\,\mathrm{GeV}^2$ in a coupled-channel approach; we require only the result on the $\pi\pi$ cut for $t < 1\,\mathrm{GeV}^2$. Figure 7 shows the normalized squared modulus of the FF, $|\sigma_\pi(t)|^2/M_\pi^4$, as it enters in the dispersive improvement formula Eq. (17). One sees that it reaches a value $\sim$3 at $t \sim 0.3\,\mathrm{GeV}^2$, which indicates the presence of strong $\pi\pi$ rescattering. This underscores the rationale for our approach, as it would be very difficult to incorporate these effects through higher order chiral corrections.

The overall uncertainty of the nucleon spectral function calculated in our approach is determined by the uncertainty of the χEFT calculation of $J^0_+(t)$ and the uncertainty of the empirical $\sigma_\pi(t)$. In the numerical results presented in the following, we show only the uncertainties resulting from the χEFT calculation of $J^0_+(t)$, which can be quantified within our approach.

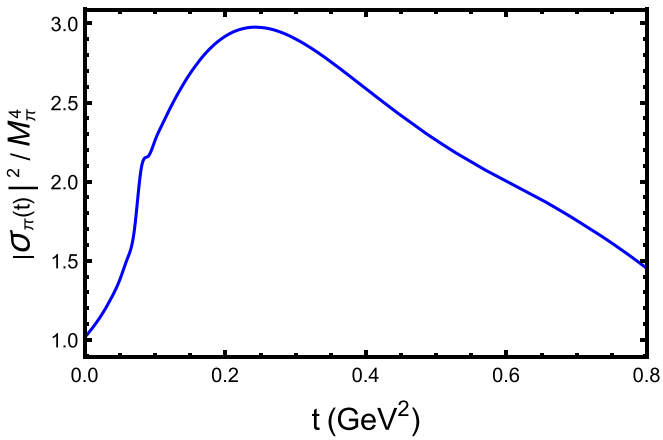

FIG. 7. Pion scalar FF obtained in the dispersive analysis of Ref. [35]. The plot shows the normalized squared modulus of the FF, $|\sigma_\pi(t)|^2/M_\pi^4$, as it enters in the improvement formula Eq. (17).

III. RESULTS

A. Nucleon scalar spectral function

We now present the results of the dispersively improved χEFT calculation of the scalar FF with the methods described in Sec. II. Figure 8 shows the function $J^0_+(t)$, Eq. (16), which is the primary object of the χEFT calculation (cf. Fig. 5). One observes the following:

(a) The chiral expansion shows good convergence. Higher order corrections are small at the threshold and become increasingly important at larger t. NLO corrections from the LECs give a strong positive contribution at $t > 0.5\,\mathrm{GeV}^2$ (mainly due to the contribution of c_3), which is corrected downward by the N2LO corrections estimated according to Sec. II C. As a consequence, the NLO+N2LO results are close to the LO over a wide range of t.

(b) The χEFT predictions agree well with the dispersion-theoretical result of Ref. [70], obtained by analytic continuation of the $\pi\pi \to N\bar{N}$ PWA extracted from πN scattering data. The LO χEFT result describes the dispersion-theoretical result very close to threshold. The NLO corrections improve the behavior in the near-threshold region and lead to agreement with the dispersion-theoretical result up to $t \lesssim 0.2\mathrm{GeV}^2$, but are too large at larger t. Finally, the N2LO estimate reproduces the dispersion-theoretical result over the entire range up to $t \sim 0.8\mathrm{GeV}^2$.

These observations provide strong justification for our program of applying χEFT to the real function $J^0_+(t)$, including the approximate treatment of N2LO corrections (see Sec. II C). The convergence pattern observed here directly carries over to the spectral function $\mathrm{Im}\,\sigma(t)$.

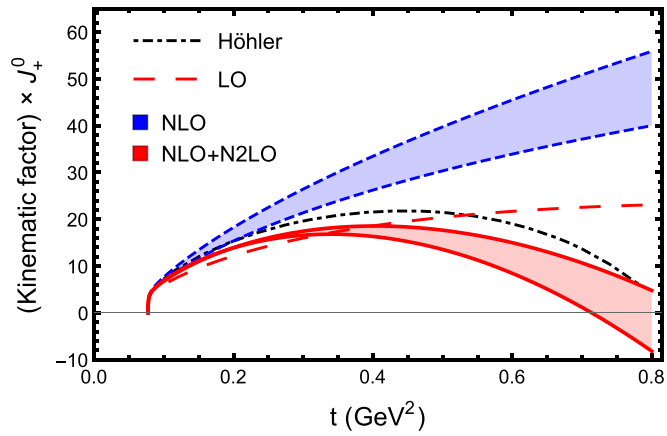

FIG. 8. χEFT results for the function $3k_{\mathrm{cm}}/(4\widetilde{p}_N^2\sqrt{t})\,J^0_+(t)$, which enters in the manifestly real unitarity relation Eq. (15). Long-dashed red line: LO. Blue band with short-dashed contours: NLO. Red band with solid contours: NLO + N2LO, estimated as described in Sec. II C. (The bands labeled NLO and NLO+N2LO show the total result up to that order and include the LO contribution.) Dash-dotted black line: Dispersion-theoretical result of Ref. [70].

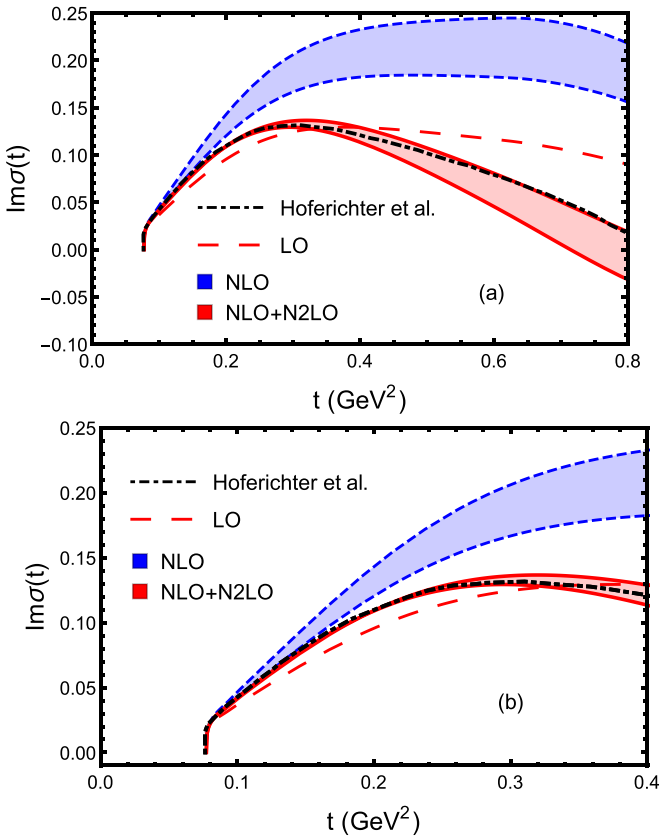

FIG. 9. DIχEFT results for the scalar spectral function, Eq. (17). The upper plot (a) covers the full range up to $t = 0.8\,\mathrm{GeV}^2$; the lower plot (b) covers the near-threshold region. The long-dashed red lines (LO approximation), blue bands with short-dashed contours (NLO), and red bands with solid contours (NLO+N2LO) correspond to those of Fig. 8. Dash-dotted black lines: Roy-Steiner result of Ref. [19].

Figure 9 shows our predictions for the scalar spectral function $\mathrm{Im}\,\sigma(t)$, obtained by multiplying the χEFT results for $J^0_+(t)$ with the empirical $|\sigma_\pi(t)|^2$, Eq. (15). Also shown is the spectral function obtained from a recent analysis using Roy-Steiner equations [19].[1] One observes that the LO χEFT result is in reasonable agreement with the Roy-Steiner result up to energies $t \sim 0.3\,\mathrm{GeV}^2$. The NLO correction improves the near-threshold behavior but overestimates the spectral function at intermediate energies. The N2LO corrections, estimated according to Sec. II C, have the right t dependence to correct this issue. Altogether we obtain excellent agreement with the Roy-Steiner result up to $t \sim 1\,\mathrm{GeV}^2$.

B. Nucleon scalar radius

With the DIχEFT result for the spectral function, we can now compute the nucleon scalar radius, using the well-convergent dispersion integral Eq. (7). Table I shows the results obtained with different values of $\sigma(0)$. Note that $\sigma(0)$ enters directly in the normalization factor, Eq. (7), and indirectly through the procedure fixing the N2LO parameters (see Sec. II C). One observes that the nucleon scalar radius is substantially larger than the charge radius (Dirac radius), $\langle r^2\rangle_\sigma > \langle r^2\rangle_1 \sim 0.65\,\mathrm{fm}^2$, as pointed out in Ref. [17].

TABLE I. Nucleon scalar radius obtained in DIχEFT with different values of $\sigma(0)$. (A) $\sigma(0) = 59$ MeV; (B) 45 MeV.

		LO	NLO	NLO+N2LO
$\langle r^2\rangle_\sigma$ (fm^2)	A	1.06	1.40–1.67	1.03–1.13
	B	1.38	1.83–2.19	1.34–1.49

It is interesting to compare our results for the scalar radius with those of the dispersion-theoretical calculation of Ref. [17], not the least because the DIχEFT calculation can provide systematic uncertainty estimates. We find that, at NLO+N2LO accuracy, our radius calculated with $\sigma(0) = 45$ MeV is smaller than that of Ref. [17], which uses the same value of $\sigma(0)$. The difference can be traced back to the spectral function, which in our calculation comes out smaller than that of Ref. [17] in the near-threshold region. We note that the DIχEFT result agrees with that of the Roy-Steiner analysis of Ref. [19]. The latter provides a value of $\langle r^2\rangle_\sigma = 1.07(4)$ fm^2 when $\sigma(0) = 59$ MeV is used [71], in excellent agreement with what we obtain.

C. Nucleon scalar form factor

Using the once-subtracted dispersion relation Eq. (4), we can also calculate the t-dependent scalar FF, both in the region below threshold $t < 4M_\pi^2$ (where it is real) and above threshold $t > 4M_\pi^2$ (where it is complex). Figure 10 shows the results obtained with the DIχEFT spectral functions at different orders, along with the dispersion-theoretical result of Ref. [17]. In order to suppress the dependence on the uncertain $\sigma(0)$ the figure shows the difference $\sigma(t) - \sigma(0)$ instead of $\sigma(t)$. One observes that the DIχEFT calculations converge well, especially at $t < 4M_\pi^2$. The LO approximation already gives a result in good agreement with the dispersive one. The NLO contribution corrects the LO result in the right direction, but by too much in magnitude; this is because it overestimates the spectral function in the intermediate-t region, which still has some modest influence on the result of the dispersion integral for the FF. At NLO+N2LO, once we enforce that the dispersion integral reproduce the chosen $\sigma(0)$ (see Sec. II C), the DIχEFT scalar FF is in excellent agreement with the dispersion-theoretical one.

D. Cheng-Dashen discrepancy

Table II gives the results for the Cheng-Dashen discrepancy Eq. (6) in DIχEFT, calculated through the dispersion integral Eq. (8). One observes the same pattern of convergence as in the scalar radius and the FF: The NLO corrections are strongly positive and the N2LO corrections are negative, such

[1] We compare our results for $J^0_+(t)$ with the dispersion-theoretical analysis of Ref. [70], which is based on old data but quotes results directly for this real function. Our results for $\mathrm{Im}\,\sigma(t)$ we instead compare with the Roy-Steiner analysis of Ref. [19], which is based on the most recent $\pi\pi$ and πN scattering data.

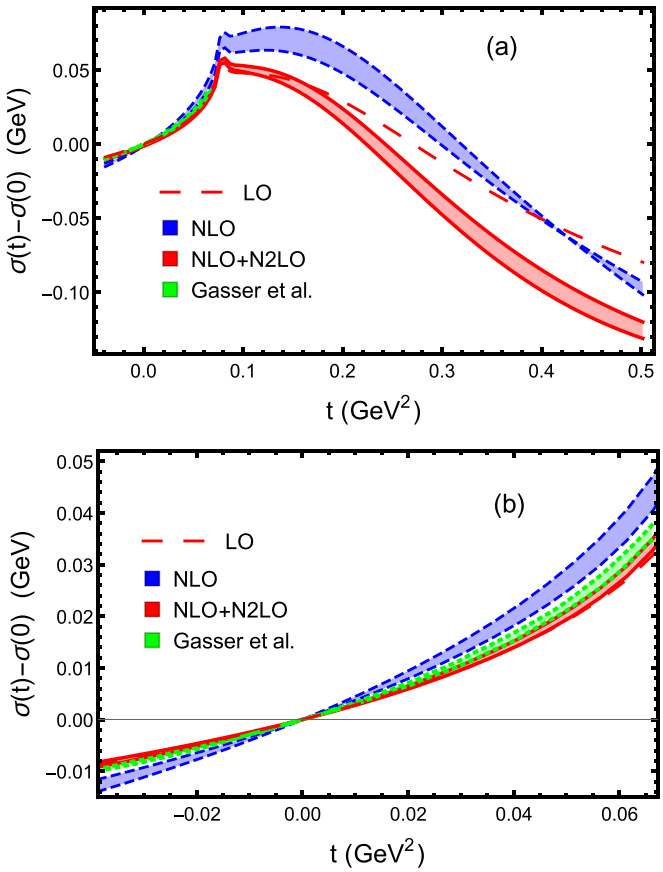

FIG. 10. Real part of the nucleon scalar FF $\Delta\sigma(t) = \sigma(t) - \sigma(0)$, obtained from the once-subtracted dispersion integral Eq. (4) with the DIχEFT spectral functions. The upper plot (a) shows the full t-range up to 0.5 GeV^2, the lower plot (b) the near-threshold region. The long-dashed red lines (LO approximation), blue bands with short-dashed contours (NLO), and red bands with solid contours (NLO+N2LO) correspond to those of Figs. 8 and 9. Green bands with dotted contours: Dispersion-theoretical result of Ref. [17].

that the total result at N2LO is rather close to the original LO one.

The Cheng-Dashen discrepancy has been computed previously using different methods. The first χEFT calculation was reported in Ref. [25] and obtained $\Delta_\sigma = 4.6$ MeV at $\mathcal{O}(p^3)$ accuracy. The dispersive analysis of Ref. [17] then obtained a much larger value, $\Delta_\sigma = 15.2(4)$ MeV, pointing to the inability of χEFT to generate sufficient curvature in $\sigma(t)$ at $\mathcal{O}(p^3)$ accuracy (according to the the same reference, this has almost no effect on the extraction of the σ term from πN scattering data). The curvature necessary to recover the dispersive result was obtained in an $\mathcal{O}(p^4)$ calculation in Ref. [72], which found $\Delta_\sigma = 14.0\,\text{MeV} + 2M_\pi^4 \bar{e}_2$. This larger value was supported by an updated dispersive calculation in Ref. [19], which finds $\Delta_\sigma = 13.9(3)$ MeV. The DIχEFT approach described here gives results in excellent agreement with the dispersive calculation. The main improvement compared to conventional χEFT is that it includes the strong $\pi\pi$ rescattering effects. It is interesting that such effects are essential even at $t = 2M_\pi^2$, which should be well within the radius of convergence of conventional χEFT calculations.

TABLE II. DIχEFT results for the Cheng-Dashen discrepancy Δ_σ, Eq. (6).

	LO	NLO	NLO+N2LO
Δ_σ (MeV)	13.3	17.4 - 20.6	13.3 - 14.5

IV. DISCUSSION

A. Euclidean correlation functions

The DIχEFT approach incorporates $\pi\pi$ rescattering effects in the nucleon spectral functions through the timelike pion FF, which is provided by sources outside of χEFT. An important aspect is that the pion FF enters only through its squared modulus, so that knowledge of its phase is not required [see Eq. (15)]. The modulus of the pion timelike FF can in principle be extracted from the vacuum correlation function of the operator, which can be continued to imaginary time (Euclidean QCD) and evaluated using nonperturbative methods such as lattice QCD. This opens up the interesting possibility of combining the χEFT calculations of the $\pi\pi \to N\bar{N}$ amplitude with Euclidean QCD calculations of the pion timelike FF. Here we describe this connection for the scalar operator; the expressions can easily be generalized to other G-parity-even operators.

The vacuum polarization induced by the scalar density operator Eq. (1) is given by the two-point correlation function [73–75]

$$\Pi_\sigma(q^2) \equiv i \int d^4x e^{iqx} \langle 0|\, \mathrm{T}\, O_\sigma(x) O_\sigma(0)\, |0\rangle, \qquad (19)$$

where x is a 4-dimensional Minkowskian space-time displacement, T denotes the time-ordering operation, and the 4-momentum q can be spacelike or timelike, $q^2 < 0$ or > 0. $\Pi_\sigma(q^2)$ is an analytic function of q^2, with no singularities at $q^2 < 0$ and cuts at $q^2 > 0$, corresponding to hadronic intermediate states produced by the operator O_σ. The function obeys subtracted dispersion relations of the form [$\Pi_\sigma^{(k)}(q^2)$ denotes the kth derivative with respect to q^2],

$$\Pi_\sigma(q^2) - \sum_{k=0}^{n-1} (q^2)^k \frac{\Pi_\sigma^{(k)}(0)}{k!} = \frac{(q^2)^n}{\pi} \int_{4M_\pi^2}^{\infty} dt' \frac{\mathrm{Im}\,\Pi_\sigma(t')}{(t')^n (t' - q^2)}, \qquad (20)$$

where $n \geqslant 2$ for the scalar operator, based on the expected short-distance behavior of the coordinate-space correlation function. The imaginary part is proportional to the cross section for hadron production by the scalar operator at the squared mass t' and is positive, $\mathrm{Im}\,\Pi_\sigma(t') > 0$. In the region $4M_\pi^2 < t' < 16M_\pi^2$, the only accessible hadronic state is the $\pi\pi$ state (two-pion cut). The imaginary part on the two-pion cut is given by an elastic unitarity formula analogous to Eq. (12), with the pion FF appearing both in the initial (operator $\to \pi\pi$) and the final ($\pi\pi \to$ operator) amplitudes

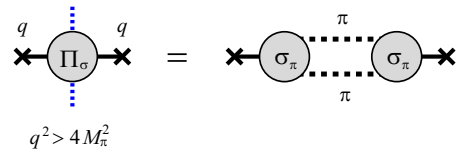

FIG. 11. Two-pion cut of the scalar correlation function, Eq. (21).

(see Fig. 11),

$$\mathrm{Im}\,\Pi_\sigma(t') = \frac{k_{\rm cm}}{8\pi\sqrt{t}}|\sigma_\pi(t')|^2 \quad \left(4M_\pi^2 < t' < 16M_\pi^2\right). \tag{21}$$

It provides a direct connection between the squared modulus $|\sigma_\pi(t')|^2$ and the vacuum correlation function.

In order to put Eq. (21) to practical use, one must have a method to extract the imaginary part on the two-pion cut from (approximate) calculations of the correlation function, Eq. (19). Here one may use the fact that the lowest-mass state in the spectral representation determines the asymptotic behavior of the coordinate-space correlation function at large spacelike distances. Substituting the spectral representation Eq. (20) of $\Pi_\sigma(q^2)$ in Eq. (19) and inverting the Fourier transform, one obtains a spectral representation of the coordinate-space function at spacelike distances,[2]

$$\begin{aligned}&\langle 0|\,\mathrm{T}\,O_\sigma(x)O_\sigma(0)\,|0\rangle \\ &= \int_{4M_\pi^2}^{\infty} dt' \frac{\sqrt{t'}\,K_1(\sqrt{t'}\sqrt{-x^2})}{4\pi^2\sqrt{-x^2}}\mathrm{Im}\,\Pi_\sigma(t') \quad (x^2 < 0).\end{aligned} \tag{22}$$

The modified Bessel function decays exponentially at large arguments, $K_1(z) \sim [\pi/(2\sqrt{z})]^{1/2}\exp(-z)$ for $z \gg 1$. For a given distance $\sqrt{-x^2}$, the factor $K_1(\sqrt{t'}\sqrt{-x^2})$ strongly suppresses the contribution from energies $\sqrt{t'} \gg 1/\sqrt{-x^2}$ in Eq. (22). The asymptotic behavior of the coordinate-space function is therefore dominated by t' in the vicinity of the two-pion threshold in the spectral integral; it is of the form $\sim\exp(-2M_\pi\sqrt{-x^2})P(-x^2)$, where the pre-exponential factor P depends on the threshold behavior of $\mathrm{Im}\,\Pi_\sigma(t')$, Eq. (21). At large but finite distances, the spectral integral Eq. (22) extends over the entire two-pion cut, with exponential suppression of higher mass states. Whether this representation could be used to extract quantitative information on $|\sigma_\pi(t')|^2$ from lattice QCD calculations of the coordinate-space correlation function at distances $\sqrt{-x^2} \sim 1/M_\pi$ is an interesting question for further study. The success of this program depends on the contribution of higher mass states with $t' > 16\,M_\pi^2$ to the spectral integral, which could be inferred from the lattice QCD calculations of the correlator at shorter distances or estimated using quark-hadron duality.

[2]In deriving Eq. (22), one may disregard the subtractions in Eq. (20) and consider the Fourier transform of the formal unsubtracted dispersion integral with $n = 0$. The subtraction terms result in δ functions at $x = 0$, or derivatives thereof, which can be neglected when considering the behavior of the coordinate-space correlation function at finite distances.

The timelike pion FF at $4M_\pi^2 < t < 16M_\pi^2$ can also be computed in lattice QCD using a variant of the Lüscher method, which exploits the correspondence between the $\pi\pi$ scattering phase shift and the energy levels of the $\pi\pi$ system in a finite volume [76]. Again this method delivers the squared modulus of the timelike pion FF without determining the phase. Results for $|\sigma_\pi(t')|^2$ obtained with either of the methods described here could be incorporated into our DIχEFT approach through Eq. (15).

B. Connection with large-N_c QCD

It is worthwhile to investigate the connection of our approach with the large-N_c limit of QCD. This exercise shows that the DIχEFT results obey the general N_c-scaling relations for the scalar FF and explains the relative contribution of N and Δ intermediate states in the chiral processes.

The limit of a large number of colors is a powerful method for connecting properties of mesons and baryons with the microscopic theory of strong interactions [77–79]; see Ref. [80] for a review. While the dynamics remains complex and cannot be solved exactly, the scaling behavior of meson and baryon properties with N_c can be established on general grounds and provides insights into their structure and guidance for the formulation of effective theories. The masses of low-lying mesons scale as $\mathcal{O}(N_c^0)$; the masses of baryons scale as $\mathcal{O}(N_c)$ for states with spin-isospin $\mathcal{O}(N_c^0)$; while the hadronic size of mesons and baryons is $\mathcal{O}(N_c^0)$ and remains stable in the large-N_c limit. Baryons thus are heavy objects of finite size, whose external motion in coordinate and isospin-spin space can be described classically, with a mass and moment of inertia of $\mathcal{O}(N_c)$. The N and Δ are the rotational states of the classical body with isospin-spin $I = J = 1/2$ and $3/2$, and the mass splitting is $m_\Delta - m_N = \mathcal{O}(N_c^{-1})$. Further scaling relations can be obtained for the matrix elements of QCD operators between meson and baryon states, and the meson-meson and meson-baryon couplings. The relations are model independent and can be derived in many different ways: diagrammatic arguments [78], group-theoretical methods [81,82], large-N_c quark models [83,84], and the soliton picture of baryons [85,86].

The N_c scaling of the nucleon's scalar FF considered in the present study can be established as follows. The standard techniques show that the nucleon σ term scales as $\sigma(0) = \mathcal{O}(N_c)$. This is plausible because the σ term represents the response of the nucleon mass to a change of the QCD quark mass, $\sigma(0) = \hat{m}(\partial/\partial\hat{m})m_N$. Since the nucleon's spatial size is $\mathcal{O}(N_c^0)$, we consider the scalar FF at nonexceptional momentum transfers $|t| = \mathcal{O}(N_c^0)$, in either the spacelike or timelike domain. For such values of t, the scaling behavior of the FF is then given by

$$\sigma(t) = \mathcal{O}(N_c) \quad [|t| = \mathcal{O}(N_c^0)]. \tag{23}$$

Because $M_\pi = \mathcal{O}(N_c^0)$, the t region of elastic unitarity ($4M_\pi^2 < t < 16M_\pi^2$) remains stable in the large-N_c limit. Thus the basic setup of our dispersive analysis remains stable in the large-N_c limit: The dispersion integral extends over momenta $t = \mathcal{O}(N_c^0)$ and converges in that parametric domain, and we require the spectral function at energies $t = \mathcal{O}(N_c^0)$. For the

pion scalar FF, the same arguments lead to $\sigma_\pi(0) = M_\pi^2 = \mathcal{O}(N_c^0)$ and therefore

$$\sigma_\pi(t) = \mathcal{O}(N_c^0) \quad \big[|t| = \mathcal{O}(N_c^0)\big]. \tag{24}$$

Equations (23) and (24) imply that the scalar FF of the hadrons scales with the number of their valence quarks, as one would expect in a "constituent quark" picture of dynamical chiral symmetry breaking.

It is easy to verify the that the DIχEFT results for the scalar nucleon FF obey the general N_c scaling of Eq. (23). Using the explicit expression Eq. (A2) with $g_A = \mathcal{O}(N_c)$ and $f_\pi = \mathcal{O}(\sqrt{N_c})$, one finds that the contribution of the N Born term to $J_+^0(t)$ scales as

$$J_+^0(t)[\mathrm{LO},N] = \mathcal{O}(N_c^3) \quad \big[|t| = \mathcal{O}(N_c^0)\big]. \tag{25}$$

Using Eq. (A5) with $h_A = \mathcal{O}(N_c)$, one finds the same scaling behavior for the contribution of the Δ Born term.[3] Multiplication with $|\sigma_\pi(t)|^2$, Eq. (24), does not change this scaling behavior. Taking into account the scaling behavior of the kinematic factor in Eq. (12), one concludes that the DIχEFT result for the spectral function scales according to Eq. (23). This scaling behavior then carries over to the FF through the dispersion relation Eq. (4).

It is interesting to compare the relative contributions of the N and Δ Born terms to the scalar spectral function in the large-N_c limit. In the large-N_c limit, the N and Δ become degenerate, $\{m_N, m_\Delta\} = \mathcal{O}(N_c)$ and $m_\Delta - m_N = \mathcal{O}(N_c^{-1})$, and the πNN and $\pi N\Delta$ couplings are related by [85]

$$g_{\pi N\Delta} = \tfrac{3}{2} g_{\pi NN} \quad (N_c \to \infty). \tag{26}$$

Both statements follow from the fact that the N and Δ are rotational states of a classical body with combined isospin-spin symmetry. The conventional couplings of Eq. (26) are related to the χEFT couplings by

$$g_{\pi NN} = \frac{g_A m_N}{f_\pi}, \quad g_{\pi N\Delta} = \frac{h_A m_N}{\sqrt{2} f_\pi}, \tag{27}$$

and scale as $\{g_{\pi NN}, g_{\pi N\Delta}\} = \mathcal{O}(N_c^{3/2})$. Using Eqs. (26) and (27) and the expressions in the appendix, one easily shows that the LO χEFT results satisfy

$$\mathrm{Im}\,\sigma(t)[\mathrm{LO},\Delta] = 2\,\mathrm{Im}\,\sigma(t)[\mathrm{LO},N] \quad (N_c \to \infty); \tag{28}$$

i.e., the contribution of the Δ Born term is twice as large as that of the N one. Such behavior was observed in earlier χEFT calculations of the nucleon's scalar structure [87,88]. It was also seen in studies of the nucleon's peripheral gluon and singlet quark structure, which are measured by operators with the same isospin-spin quantum numbers as the scalar density [89,90].

[3]Equation (25) is valid for $k_{\mathrm{cm}}^2 = t/4 - M_\pi^2 = \mathcal{O}(N_c^0)$, i.e., for nonexceptional values $t = \mathcal{O}(N_c^0)$, not parametrically close to the two-pion threshold. In this case, $\{x_N, x_\Delta\} = \mathcal{O}(N_c^{-1})$ in Eqs. (A3) and (A6), and the inverse tangent functions in Eqs. (A2) and (A5) count as $\arctan\{x_N, x_\Delta\} \approx \pi/2 = \mathcal{O}(N_c^0)$. The polynomial terms in Eqs. (A2) and (A5) are suppressed relative to the inverse tangent terms by a power N_c^{-1}.

The relative factor in Eq. (28) can be explained in a simple manner. Consider the scalar FF in the proton isospin state, p. In the Born graph with intermediate N, the possible intermediate states are $\pi^0 p$ and $\pi^+ n$; in the Born graph with intermediate Δ, they are $\Delta^{++}\pi^-, \Delta^+\pi^0$, and $\Delta^0\pi^+$. The Lagrangian with the relevant πNN and $\pi N\Delta$ couplings is

$$\begin{aligned}\mathcal{L}_{\pi NB} \propto{}& \frac{g_{\pi NN}}{2}(\sqrt{2}\bar{p}n\pi^+ + \bar{p}p\pi^0) \\ &+ \frac{g_{\pi N\Delta}}{3}(\sqrt{3}\bar{p}\Delta^{++}\pi^- + \sqrt{2}\bar{p}\Delta^0\pi^0 + \bar{p}\Delta^0\pi^+) \\ &+ (\mathrm{H.c.}),\end{aligned} \tag{29}$$

where we display only the isospin structure and omit the dependence on the pion momentum (for the full structure, see Ref. [91] and references therein). Each pion state contributes equally to the scalar charge; cf. Eq. (9). The relative contribution of the N and Δ Born graphs is therefore given by the sum of the squared couplings in Eq. (29),

$$\mathrm{Im}\,\sigma(t)[\mathrm{LO},N] \propto \frac{g_{\pi NN}^2}{4}(2+1) = \frac{3g_{\pi NN}^2}{4}, \tag{30}$$

$$\mathrm{Im}\,\sigma(t)[\mathrm{LO},\Delta] \propto \frac{g_{\pi N\Delta}^2}{9}(3+2+1) = \frac{2g_{\pi N\Delta}^2}{3}. \tag{31}$$

With the large-N_c relation between the couplings, Eq. (26), one then obtains the relative factor of Eq. (28).

The observation of Eq. (28) represents one instance of a general phenomenon in χEFT: In the large-N_c limit the contributions of N and Δ intermediate states are related by a simple factor, and their sum produces a result that exhibits the correct N_c scaling established on general grounds. Note that the factor between the N and Δ contributions depends on the isospin-spin quantum numbers of the operator and the matrix element [87,88]. For the scalar operator considered here, the individual N and Δ contributions already have the correct N_c scaling, and summing them just increases the coefficient compared to N only. In the case of the isovector-vector FFs (Dirac and Pauli), the individual N and Δ contributions have incorrect N_c scaling—their scaling exponents are too large by one power of N_c—and summing them is necessary in order to cancel the leading term and recover the correct general N_c scaling [87,88,91,92].

The large-N_c relation Eq. (28) represents an important theoretical constraint on our χEFT calculation of scalar nucleon structure. Confronting the large-N_c prediction with the actual χEFT results for $J_+^0(t)$ obtained with the physical N and Δ masses and couplings, Fig. 5, we observe the following: (a) The actual N and Δ contributions have the same sign, in agreement with the large-N_c predictions. (b) The magnitude of the actual Δ contribution is significantly smaller than the large-N_c prediction, amounting to $\sim 1/2$ rather than 2 times the N contribution. This demonstrates that $1/N_c$ suppressed terms play an essential role in the χEFT result for $J_+^0(t)$. Notice that the large-N_c limit corresponds to the heavy-baryon limit of χEFT because $M_\pi/m_N = \mathcal{O}(N_c^{-1})$; it is known that the heavy-baryon expansion converges poorly for the spectral functions on the two-pion cut; see Refs. [27,92] for a discussion.

V. OUTLOOK

We have presented a general method for calculating the nucleon FFs of G-parity-even operators by combining χEFT and dispersion theory. The spectral functions on the two-pion cut are constructed with the help of the elastic unitarity condition, using a manifestly real representation that separates the coupling of the $\pi\pi$ system to the nucleon from the $\pi\pi$ rescattering (N/D method). χEFT is used to calculate the real function describing the $\pi\pi$ coupling to the nucleon, which is free of $\pi\pi$ rescattering effects. It is dominated by the LO Born amplitudes with N and Δ intermediate states and shows good convergence in higher orders. The effects of $\pi\pi$ rescattering are then incorporated by multiplying with the squared modulus of the timelike pion FF, which can be determined empirically or extracted from lattice QCD calculations of the vacuum correlation function of the operator. Our method represents a major improvement over traditional χEFT calculations of the spectral functions, which try to account for the $\pi\pi$ rescattering effects through χEFT interactions. It permits calculations of nucleon spectral functions up to $t \sim 1\,\mathrm{GeV}^2$ (details depend on the operator) and opens up the prospect of a realistic dispersive analysis of nucleon FFs and related quantities based on χEFT.

We have applied the method to the nucleon scalar FF. The χEFT calculations of the real function $J^0_+(t)$ show good convergence and are in excellent agreement with dispersion-theoretical results up to $t \sim 0.8\,\mathrm{GeV}^2$. This information is sufficient for evaluating the t dependence of the scalar FF, the scalar radius, and the Cheng-Dashen discrepancy, through a once-subtracted dispersion relation. Our calculation determines the scalar FF at momentum transfers up to $|t| \sim 0.5\,\mathrm{GeV}^2$ with controlled uncertainties. The nucleon's scalar FF is of principal interest for understanding the role of dynamical chiral symmetry breaking in nucleon structure and the origin of the nucleon mass. It is also an ingredient in modeling the interaction of dark matter with the nucleon for the purpose of designing direct detection experiments [93].

The method described here can be applied to nucleon FFs of any G-parity-even operators with a two-pion cut. Applications to the nucleon isovector-vector FFs will be presented in a forthcoming article [36]. Other possible applications are the nucleon FFs of the energy-momentum tensor and the moments of generalized parton distributions; see Ref. [94] for a recent dispersive calculation. The impact of the method depends on the convergence of the χEFT calculations of the J functions and on the actual strength distribution in the dispersion integrals under study, and has to be demonstrated channel by channel. Subtractions can make the dispersion integrals more convergent and emphasize the low-t' region where the spectral functions can be computed using our method. Another attractive possibility is to consider the transverse spatial densities associated with the FFs, which are represented by exponentially convergent dispersion integrals and can safely be calculated with our method at peripheral distances $b \gtrsim 1\, M_\pi^{-1}$ [32]. An interesting question is whether the dispersive method described here could be extended to calculate the nucleon's peripheral partonic structure at fixed light-front momentum fraction x; such calculations have so far been performed in the standard χEFT approach without explicit treatment of $\pi\pi$ rescattering [89,90,95].

An obvious extension of the present calculation would be to the nucleon FFs of the scalar strange quark and gluonic operators, which have the same quantum numbers as the light-quark scalar operator, Eq. (1) [5]. The dispersive calculation of these FFs must include also the $K\bar{K}$ channel and its coupling to $\pi\pi$ in a coupled-channel approach. The extension of our method to this situation raises several interesting questions: (a) One would need to generalize the N/D method and the manifestly real representation of the unitarity condition, Eq. (15), to the case of coupled $\pi\pi$ and $K\bar{K}$ channels, and possibly other inelasticities. (b) One would need to explore how well χEFT works for the coupling of the $K\bar{K}$ system to the nucleon (octet and decuplet baryon Born terms, contact terms). (c) The distribution of strength in the dispersive integral of the strange and gluonic FF is expected to be very different from that of the light-quark scalar FF and may involve large contributions from energies $t' > 1\,\mathrm{GeV}$, where our approach is not applicable. (d) One would need a parametrization of the pion and kaon FFs of these operators that takes into account coupled-channel dynamics. Some experimental information on these FFs is available from τ lepton decays [35]. The timelike pion and kaon FFs could also be extracted from the vacuum correlation function of the respective operators, as described in Sec. IV A.

The DIχEFT approach described here could in principle also be extended to the nucleon FFs of G-parity odd operators with a 3-pion cut. Methods for implementing elastic unitarity in 3-body channels are presently being developed in connection with the analysis of meson decays [96] and the extraction of scattering phase shifts and resonance parameters from lattice QCD [97,98]. How to formulate an analog of the present N/D method for the 3-body system, and how to match the 3-body unitarity formula with χEFT calculations, are interesting problems for further study. If our method could be extended to the 3-pion cut it would open up applications to the nucleon isoscalar-vector and isovector-axial FFs, about which little is known from first principles.

ACKNOWLEDGMENTS

We thank M. Hoferichter for useful communication regarding the nucleon scalar radius and the results of Ref. [71]. This material is based upon work supported by the U.S. Department of Energy, Office of Science, Office of Nuclear Physics under Contract No. DE-AC05-06OR23177. This work was also supported by the Spanish Ministerio de Economía y Competitividad and European FEDER funds under Contract No. FPA2016-77313-P.

APPENDIX: EXPRESSIONS

For reference, we present in this appendix the LO and NLO χEFT expressions for the real function $J^0_+(t)$, Eq. (16), which are used in the analytical and numerical studies in the text. In

the following, $4M_\pi^2 < t < 4m_N^2$ and [cf. Eqs. (13) and (14)]

$$k_{\rm cm} = \sqrt{t/4 - M_\pi^2}, \quad \widetilde{p}_{\rm cm} = \sqrt{m_N^2 - t/4}. \tag{A1}$$

The contribution of the N Born diagram [Fig. 4(a)] is

$$J_+^0(t)[\mathrm{LO}, N] = \frac{g_A^2 m_N^3}{4\pi f_\pi^2 M_\pi^2}\left(\frac{\arctan x_N}{x_N} - \frac{t}{4m_N^2}\right), \tag{A2}$$

$$x_N \equiv \frac{2k_{\rm cm}\widetilde{p}_{\rm cm}}{A_N} = \frac{2\sqrt{t/4 - M_\pi^2}\sqrt{m_N^2 - t/4}}{t/2 - M_\pi^2}, \tag{A3}$$

$$A_N \equiv t/2 - M_\pi^2. \tag{A4}$$

The contribution of the Δ Born diagram [Fig. 4(b)] is

$$J_+^0(t)[\mathrm{LO}, \Delta] = \frac{h_A^2}{48\pi f_\pi^2 M_\pi^2}(C_\Delta \arctan x_\Delta + D_\Delta), \tag{A5}$$

$$x_\Delta \equiv \frac{2k_{\rm cm}\widetilde{p}_{\rm cm}}{A_\Delta} = \frac{2\sqrt{t/4 - M_\pi^2}\sqrt{m_N^2 - t/4}}{t/2 - M_\pi^2 + m_\Delta^2 - m_N^2}, \tag{A6}$$

$$A_\Delta \equiv t/2 - M_\pi^2 + m_\Delta^2 - m_N^2. \tag{A7}$$

The coefficient of the inverse tangent function in Eq. (A5) is obtained as

$$C_\Delta \equiv \frac{2\widetilde{p}_{\rm cm}^2 F - A_\Delta m_N G}{k_{\rm cm}\widetilde{p}_{\rm cm}}, \tag{A8}$$

in which

$$F \equiv \alpha(m_\Delta + m_N) + \frac{\beta}{3}(m_\Delta - m_N), \tag{A9}$$

$$G \equiv -\alpha + \frac{\beta}{3}, \tag{A10}$$

$$\alpha \equiv \frac{t}{2} - m_N^2 + \frac{\left(m_\Delta^2 + m_N^2 - M_\pi^2\right)^2}{4m_\Delta^2}, \tag{A11}$$

$$\beta \equiv \left(m_N + \frac{m_\Delta^2 + m_N^2 - M_\pi^2}{2m_\Delta}\right)^2. \tag{A12}$$

The full expression for the numerator in Eq. (A8), organized according to powers of M_π^2 and t, is

$$\begin{aligned}
&2\widetilde{p}_{\rm cm}^2 F - A_\Delta m_N G \\
&= 1/\left(48m_\Delta^2\right)\left[8m_N(m_N + m_\Delta)^4(m_N - m_\Delta)^2\right. \\
&\quad - 8m_N(m_N + m_\Delta)^2\left(3m_N^2 - 2m_N m_\Delta + 3m_\Delta^2\right)M_\pi^2 \\
&\quad - 8m_\Delta(m_N + m_\Delta)^2\left(m_N^2 - 4m_N m_\Delta + m_\Delta^2\right)t \\
&\quad + 8m_N\left(3m_N^2 + 2m_N m_\Delta + 3m_\Delta^2\right)M_\pi^4 \\
&\quad + 16m_\Delta\left(m_N^2 - m_N m_\Delta + m_\Delta^2\right)M_\pi^2 t \\
&\quad \left. - 12m_\Delta^3 t^2 - 8m_N M_\pi^6 - 8m_\Delta M_\pi^4 t\right].
\end{aligned} \tag{A13}$$

TABLE III. LECs used in the NLO contact term contribution to $J_+^0(t)$, Eq. (A15). The values were determined according to the procedure described in Sec. II C.

	c_1	c_2	c_3
LECs (GeV^{-1})	$(-0.28, -0.18)$	$(1.0, 1.2)$	$(-1.64, -0.79)$

The polynomial terms in Eq. (A5) are obtained as

$$\begin{aligned}
D_\Delta = 1/\left(18M_\Delta^2\right)&\left[6m_N(m_N + m_\Delta)^3(m_N - m_\Delta)\right. \\
&+ 4m_N\left(4m_N^2 + 3m_N m_\Delta + 3m_\Delta^2\right)M_\pi^2 \\
&- \left(19m_N^3 + 24m_N^2 m_\Delta + 9m_N m_\Delta^2 - 6m_\Delta^3\right)t \\
&- 6m_N M_\pi^4 - (m_N + 6m_\Delta)M_\pi^2 t \\
&\left. + (4m_N + 6m_\Delta)t^2\right].
\end{aligned} \tag{A14}$$

The inverse tangent function in Eqs. (A2) and (A5) contains the logarithmic singularity in t resulting from the left-hand cut of the $\pi\pi \to N\bar{N}$ PWA. This singularity corresponds to the intermediate baryon line of the diagrams going on mass shell, $s = \{m_N^2, m_\Delta^2\}$. The coefficient of the singularity is therefore determined by the πN scattering amplitude at the on-shell point. The latter is independent of the off-shell behavior of the χEFT even in the case of the intermediate Δ, where the definitions of the Δ propagator and the $\pi N\Delta$ vertices off the mass shell are generally ambiguous (for a discussion, see Refs. [32,91] and references therein). We note that the functions F and G in Eqs. (A9) and (A10) are just the invariant amplitudes of πN scattering at $t > 4M_\pi^2$ and $s = m_\Delta^2$, as defined in Eqs. (4.15) and (4.16) of Ref. [91]. The polynomial terms in Eqs. (A2) and (A5) depend on the behavior of the πN amplitude off the baryon mass shell. In the case of the Δ, they depend on the specific choice of the off-shell behavior and the vertices.

The masses and coupling constants used to evaluate the LO expressions are the standard values for the SU(2) flavor group (see Ref. [54]): $M_\pi = 139\,\mathrm{MeV}$, $f_\pi = 93\,\mathrm{MeV}$, $m_N = 939\,\mathrm{MeV}$, $g_A = 1.27$, and $m_\Delta = 1232\,\mathrm{MeV}$, $h_A = 2.85$.

The contribution to $J_+^0(t)$ arising from the NLO contact terms in the πN amplitude is

$$\begin{aligned}
&J_+^0(t)[\mathrm{NLO, contact}] \\
&= -\frac{\widetilde{p}_{\rm cm}^2}{12\pi f_\pi^2 m_N^2 M_\pi^2}\left(12c_1 M_\pi^2 m_N^2\right. \\
&\quad \left. + 2c_2\widetilde{p}_{\rm cm}^2 k_{\rm cm}^2 + 6c_3 m_N^2 A_N\right);
\end{aligned} \tag{A15}$$

cf. Eqs. (A1) and (A4). The values of the LECs $c_i (i = 1,2,3)$, determined according to the procedure described in Sec. II C, are listed in Table III.

[1] G. A. Miller, Annu. Rev. Nucl. Part. Sci. **60**, 1 (2010).
[2] M. Burkardt, Int. J. Mod. Phys. A **18**, 173 (2003).
[3] C. F. Perdrisat, V. Punjabi, and M. Vanderhaeghen, Prog. Part. Nucl. Phys. **59**, 694 (2007).
[4] V. Bernard, L. Elouadrhiri, and U. G. Meißner, J. Phys. G **28**, R1 (2002).
[5] M. A. Shifman, A. I. Vainshtein, and V. I. Zakharov, Phys. Lett. **78B**, 443 (1978).
[6] R. L. Jaffe and A. Manohar, Nucl. Phys. B **337**, 509 (1990).
[7] X. D. Ji, Phys. Rev. Lett. **78**, 610 (1997).
[8] M. V. Polyakov, Phys. Lett. B **555**, 57 (2003).
[9] K. Goeke, M. V. Polyakov, and M. Vanderhaeghen, Prog. Part. Nucl. Phys. **47**, 401 (2001).
[10] M. Diehl, Phys. Rep. **388**, 41 (2003).
[11] A. V. Belitsky and A. V. Radyushkin, Phys. Rep. **418**, 1 (2005).
[12] S. Boffi and B. Pasquini, Riv. Nuovo Cimento **30**, 387 (2007).
[13] W. R. Frazer and J. R. Fulco, Phys. Rev. **117**, 1603 (1960).
[14] W. R. Frazer and J. R. Fulco, Phys. Rev. **117**, 1609 (1960).
[15] G. Hohler and E. Pietarinen, Nucl. Phys. B **95**, 210 (1975).
[16] M. A. Belushkin, H.-W. Hammer, and U.-G. Meissner, Phys. Lett. B **633**, 507 (2006).
[17] J. Gasser, H. Leutwyler, and M. E. Sainio, Phys. Lett. B **253**, 260 (1991).
[18] M. Hoferichter, B. Kubis, J. Ruiz de Elvira, H.-W. Hammer, and U.-G. Meissner, Eur. Phys. J. A **52**, 331 (2016).
[19] M. Hoferichter, C. Ditsche, B. Kubis, and U.-G. Meissner, J. High Energy Phys. 06 (2012) 063.
[20] J. Gasser and H. Leutwyler, Ann. Phys. **158**, 142 (1984).
[21] J. Gasser and H. Leutwyler, Nucl. Phys. B **250**, 465 (1985).
[22] V. Bernard, N. Kaiser, and U.-G. Meissner, Int. J. Mod. Phys. E **4**, 193 (1995).
[23] S. Scherer, Adv. Nucl. Phys. **27**, 277 (2003).
[24] S. Scherer and M. R. Schindler, Lect. Notes Phys. **830**, 1 (2012).
[25] J. Gasser, M. E. Sainio, and A. Svarc, Nucl. Phys. B **307**, 779 (1988).
[26] V. Bernard, N. Kaiser, and U.-G. Meissner, Nucl. Phys. A **611**, 429 (1996).
[27] T. Becher and H. Leutwyler, Eur. Phys. J. C **9**, 643 (1999).
[28] B. Kubis and U.-G. Meissner, Nucl. Phys. A **679**, 698 (2001).
[29] N. Kaiser, Phys. Rev. C **68**, 025202 (2003).
[30] G. F. Chew and S. Mandelstam, Phys. Rev. **119**, 467 (1960).
[31] K. M. Watson, Phys. Rev. **95**, 228 (1954).
[32] J. M. Alarcón, A. N. Hiller Blin, M. J. Vicente Vacas, and C. Weiss, Nucl. Phys. A **964**, 18 (2017).
[33] B. Ananthanarayan, I. Caprini, G. Colangelo, J. Gasser, and H. Leutwyler, Phys. Lett. B **602**, 218 (2004).
[34] J. A. Oller and L. Roca, Phys. Lett. B **651**, 139 (2007).
[35] A. Celis, V. Cirigliano, and E. Passemar, Phys. Rev. D **89**, 013008 (2014).
[36] J. M. Alarcón and C. Weiss, arXiv:1710.06430 [hep-ph].
[37] C. Granados, S. Leupold, and E. Perotti, Eur. Phys. J. A **536**, 117 (2017).
[38] J. M. Alarcón, J. Martin Camalich, J. A. Oller, and L. Alvarez-Ruso, Phys. Rev. C **83**, 055205 (2011); **87**, 059901(E) (2013).
[39] J. A. Oller and E. Oset, Phys. Rev. D **60**, 074023 (1999).
[40] J. A. Oller, E. Oset, and A. Ramos, Prog. Part. Nucl. Phys. **45**, 157 (2000).
[41] U.-G. Meißner and J. A. Oller, Nucl. Phys. A **673**, 311 (2000).
[42] J. A. Oller and U.-G. Meissner, Phys. Lett. B **500**, 263 (2001).
[43] M. Albaladejo and J. A. Oller, Phys. Rev. C **84**, 054009 (2011).
[44] M. Albaladejo and J. A. Oller, Phys. Rev. C **86**, 034005 (2012).
[45] T. P. Cheng and R. F. Dashen, Phys. Rev. Lett. **26**, 594 (1971).
[46] J. M. Alarcon, J. Martin Camalich, and J. A. Oller, Phys. Rev. D **85**, 051503 (2012).
[47] J. Martin Camalich, L. S. Geng, J. Martin Camalich, and J. A. Oller, Phys. Lett. B **730**, 342 (2014).
[48] J. M. Alarcon, V. Lensky, and V. Pascalutsa, Eur. Phys. J. C **74**, 2852 (2014).
[49] V. Lensky, J. M. Alarcón, and V. Pascalutsa, Phys. Rev. C **90**, 055202 (2014).
[50] V. Lensky and V. Pascalutsa, Eur. Phys. J. C **65**, 195 (2010).
[51] A. N. Hiller Blin, T. Ledwig, and M. J. Vicente Vacas, Phys. Lett. B **747**, 217 (2015).
[52] A. H. Blin, T. Gutsche, T. Ledwig, and V. E. Lyubovitskij, Phys. Rev. D **92**, 096004 (2015).
[53] A. H. Blin, T. Ledwig, and M. J. Vicente Vacas, Phys. Rev. D **93**, 094018 (2016).
[54] T. Ledwig, J. Martin Camalich, V. Pascalutsa, and M. Vanderhaeghen, Phys. Rev. D **85**, 034013 (2012).
[55] L. S. Geng, J. Martin Camalich, L. Alvarez-Ruso, and M. J. V. Vacas, Phys. Rev. Lett. **101**, 222002 (2008).
[56] T. Ledwig, J. Martin Camalich, L. S. Geng, and M. J. V. Vacas, Phys. Rev. D **90**, 054502 (2014).
[57] J. M. Alarcon, J. Martin Camalich, and J. A. Oller, Ann. Phys. **336**, 413 (2013).
[58] V. Pascalutsa, Phys. Rev. D **58**, 096002 (1998).
[59] V. Pascalutsa and R. Timmermans, Phys. Rev. C **60**, 042201 (1999).
[60] V. Pascalutsa, Phys. Lett. B **503**, 85 (2001).
[61] H. Krebs, E. Epelbaum, and U.-G. Meissner, Phys. Rev. C **80**, 028201 (2009).
[62] T. R. Hemmert, B. R. Holstein, and J. Kambor, Phys. Lett. B **395**, 89 (1997).
[63] T. R. Hemmert, B. R. Holstein, and J. Kambor, J. Phys. G **24**, 1831 (1998).
[64] T. Fuchs, J. Gegelia, G. Japaridze, and S. Scherer, Phys. Rev. D **68**, 056005 (2003).
[65] V. Bernard, N. Kaiser, and U.-G. Meissner, Nucl. Phys. A **615**, 483 (1997).
[66] G. Ecker, J. Gasser, A. Pich, and E. de Rafael, Nucl. Phys. B **321**, 311 (1989).
[67] D. Siemens, J. Ruiz de Elvira, E. Epelbaum, M. Hoferichter, H. Krebs, B. Kubis, and U.-G. Meißner, Phys. Lett. B **770**, 27 (2017).
[68] J. Gasser, H. Leutwyler, and M. E. Sainio, Phys. Lett. B **253**, 252 (1991).
[69] M. Hoferichter, J. Ruiz de Elvira, B. Kubis, and U.-G. Meißner, Phys. Rev. Lett. **115**, 092301 (2015).
[70] G. Höhler, in *Pion Nucleon Scattering. Part 2: Methods and Results of Phenomenological Analyses*, Landolt-Börnstein 9b2, edited by H. Schopper (Springer, Berlin, 1983).
[71] M. Hoferichter, P. Klos, J. Menéndez, and A. Schwenk, Phys. Rev. D **94**, 063505 (2016).
[72] T. Becher and H. Leutwyler, J. High Energy Phys. 06 (2001) 017.
[73] M. A. Shifman, A. I. Vainshtein, and V. I. Zakharov, Nucl. Phys. B **147**, 385 (1979).
[74] M. A. Shifman, A. I. Vainshtein, and V. I. Zakharov, Nucl. Phys. B **147**, 448 (1979).
[75] L. J. Reinders, H. Rubinstein, and S. Yazaki, Phys. Rep. **127**, 1 (1985).

[76] H. B. Meyer, Phys. Rev. Lett. **107**, 072002 (2011).
[77] G. 't Hooft, Nucl. Phys. B **72**, 461 (1974).
[78] E. Witten, Nucl. Phys. B **160**, 57 (1979).
[79] S. R. Coleman and E. Witten, Phys. Rev. Lett. **45**, 100 (1980).
[80] E. Jenkins, Annu. Rev. Nucl. Part. Sci. **48**, 81 (1998).
[81] R. Dashen, E. Jenkins, and A. V. Manohar, Phys. Rev. D **49**, 4713 (1994); **51**, 2489(E) (1995).
[82] R. F. Dashen, E. Jenkins, and A. V. Manohar, Phys. Rev. D **51**, 3697 (1995).
[83] G. Karl and J. E. Paton, Phys. Rev. D **30**, 238 (1984).
[84] A. Jackson, A. D. Jackson, and V. Pasquier, Nucl. Phys. A **432**, 567 (1985).
[85] G. S. Adkins, C. R. Nappi, and E. Witten, Nucl. Phys. B **228**, 552 (1983).
[86] I. Zahed and G. E. Brown, Phys. Rep. **142**, 1 (1986).
[87] T. D. Cohen and W. Broniowski, Phys. Lett. B **292**, 5 (1992).
[88] T. D. Cohen, Rev. Mod. Phys. **68**, 599 (1996).
[89] M. Strikman and C. Weiss, Phys. Rev. D **69**, 054012 (2004).
[90] M. Strikman and C. Weiss, Phys. Rev. D **80**, 114029 (2009).
[91] C. Granados and C. Weiss, J. High Energy Phys. 06 (2016) 075.
[92] C. Granados and C. Weiss, J. High Energy Phys. 01 (2014) 092.
[93] F. Bishara, J. Brod, B. Grinstein, and J. Zupan, J. Cosmol. Astropart. Phys. 02 (2017) 009.
[94] B. Pasquini, M. V. Polyakov, and M. Vanderhaeghen, Phys. Lett. B **739**, 133 (2014).
[95] C. Granados and C. Weiss, J. High Energy Phys. 07 (2015) 170.
[96] M. Mai, B. Hu, M. Doring, A. Pilloni, and A. Szczepaniak, Eur. Phys. J. A **53**, 177 (2017).
[97] R. A. Briceño, M. T. Hansen, and S. R. Sharpe, EPJ Web Conf. **137**, 05004 (2017).
[98] R. A. Briceño, J. J. Dudek, and R. D. Young, arXiv:1706.06223 [hep-lat].